Polymer 231 (2021) 124141

Contents lists available at ScienceDirect

Polymer

journal homepage: www.elsevier.com/locate/polymer

Reversible mesophase in stress-annealed poly(3-hydroxybutyrate) fibers: A synchrotron x-ray and polarized ATR-FTIR study

E. Perret [a,b,*], K. Sharma [a,c], S. Tritsch [a,d], R. Hufenus [a]

[a] Laboratory for Advanced Fibers, Empa, Swiss Federal Laboratories for Materials Science and Technology, Lerchenfeldianum 5, 9014, St. Gallen, Switzerland
[b] Center for X-ray Analytics, Empa, Swiss Federal Laboratories for Materials Science and Technology, Überlandstrasse 129, 8600, Dübendorf, Switzerland
[c] KTH Royal Institute of Technology, Stockholm, 114 16, Sweden
[d] Hochschule Reutlingen, Alteburgstrasse 150, 72762, Reutlingen, Germany

ARTICLE INFO

Keywords:
Mesophase
poly(3-hydroxybutyrate)
P3HB
Polarized ATR-FTIR
WAXD

ABSTRACT

Structural changes in poly(3-hydroxybutyrate) (P3HB) monofilaments (diameter ~90 μm), induced by annealing under tensile stress (1 h with 1.6–40 MPa loading at 80–130 °C) have been investigated with synchrotron wide-angle x-ray diffraction (WAXD) and polarized attenuated total reflection Fourier transform infrared (ATR-FTIR) spectroscopy. Melt-spun P3HB fibers consist of an amorphous phase, a crystalline α-phase and a mesophase. Specific IR bands in *s*-polarized (electric field vector along the fiber axis) spectra have been identified to arise from the mesophase. For fibers annealed at low stress (1.6 MPa), the mesophase content practically disappears but can be recovered with tensile drawing. In-situ WAXD and polarized ATR-FTIR studies, performed during cyclic tensile loading/unloading, have revealed that the mesophase formation/dissolution is highly reversible in fibers annealed at low stress. This reversibility behavior, and the lack of off-axis reflections in WAXD patterns, support the theory that the mesophase is made of conformationally disordered and stretched chains, which are mainly located in-between α-crystals.

1. Introduction

Poly(3-hydroxybutyrate) (P3HB) is a thermoplastic biodegradable polymer, which is synthesized by microorganisms as intracellular organic inclusion. Due to its biodegradability, it is of specific interest for biomedical applications like tissue engineering, sutures or wound dressing, amongst others [1–6]. In order to tailor the mechanical properties of P3HB fibers, it is essential to understand how processing parameters and annealing parameters influence their structure, and thus their performance [7]. In the past, wide-angle x-ray diffraction (WAXD) experiments on stretched P3HB films or fibers have revealed three distinct phases: a crystalline α-phase, a mesophase and an amorphous phase [8,9]. The crystalline α-phase consists of an orthorhombic unit cell, in which two antiparallel helical P3HB chains are packed [10]. This crystalline phase gives rise to many sharp reflections in the WAXD patterns. Additionally, two rather broad equatorial peaks are observed in WAXD patterns, which cannot be attributed to the α-phase. These peaks have been thought to arise, either from A) a non-crystalline mesophase (P_{nc}), where the chains are stretched, highly-oriented and conformationally disordered [8,9,11,12], or B) from a phase made of highly-oriented chains that have a planar zigzag conformation (*β*-form) [13–16], or C) from a crystalline hexagonal *β*-form phase [17]. In our recent publication, we give an overview of mesophases that have been found in a variety of polymer fibers, and we put forward a fitting algorithm of 2D WAXD patterns [12]. In the literature, the question if the *β*-form phase in P3HB, B), is of crystalline or non-crystalline nature, has seldom been discussed in detail. A crystalline phase is expected to give rise to additional reflections, e.g., above the first layer line and on the meridian, as previously seen in WAXD patterns of highly stretched P3HB films [17,18]. Note that (as-produced) P3HB films, that are subjected to low strain (e.g. 10%), show no off-axis reflections in WAXD patterns, but only broad equatorial reflections [17]. This may indicate that a mesophase is formed at low stresses. Although the mesophase may become crystalline in highly-stretched P3HB films, it is still debatable if the phase in melt-spun P3HB fibers is crystalline or non-crystalline.

In our previous publications on melt-spun P3HB monofilaments, we have shown i) that additives can enhance the spinnability of P3HB fibers [11], ii) that the transformation of the mesophase from and into the

* Corresponding author. Laboratory for Advanced Fibers, Empa, Swiss Federal Laboratories for Materials Science and Technology, Lerchenfeldstrasse 5, 9014, St. Gallen, Switzerland.
E-mail address: edith.perret@empa.ch (E. Perret).

https://doi.org/10.1016/j.polymer.2021.124141
Received 6 July 2021; Received in revised form 25 August 2021; Accepted 26 August 2021
Available online 26 August 2021

α-form phase is partially reversible under cyclic tensile loading for unannealed (original) fibers [9], and iii) that the mesophase disappears upon annealing with low stress and recovers upon drawing [8]. In the latter study, we have also investigated the effect of annealing temperature and applied stress on the mechanical performances of the fibers, observing a viscoelastic behavior for fibers annealed at low stress. The results shown in our previous publications led us to the conclusion that the mesophase can be attributed to a non-crystalline highly oriented mesophase (P_{nc}) that is trapped between α-crystals. It has been shown that the α-crystals partially transform into the mesophase when stress is applied without heating, and that the transformation is highly reversible. This reversibility suggests that tie-molecules in-between crystals, molecules from the amorphous phase, as well as part of the chains from the α-crystals, become stretched when applying a high stress. They also retract when released, similar to the behavior of a spring.

The present work is a continuation of our previous articles [8,9,11], and we are addressing the following open questions: (a) Can mesophase off-axis reflections be detected in WAXD patterns of our melt-spun P3HB fibers? (b) How does the mesophase content depend on the annealing conditions (temperature and stress)? (c) Is the mesophase formation/dissolution of fibers, annealed at low stress, reversible during cyclic tensile drawing, and how does it depend on the annealing temperature?

To answer the first two questions (a, b), we have measured synchrotron wide-angle x-ray diffraction (WAXD) patterns of differently stress-annealed P3HB fibers. To answer question (c), we have measured in-situ synchrotron WAXD patterns, as well as polarized attenuated total reflection Fourier transform infrared (ATR-FTIR) spectra during cyclic tensile drawing of P3HB fibers annealed at low stress. Polarized ATR-FTIR spectra have been measured in order to verify if specific IR bands also show a reversible behavior during cyclic tensile drawing.

2. Experimental

2.1. Melt-spinning of P3HB fibers

Two P3HB fibers were melt-spun from modified P3HB (density 1.2 g/cm^3), provided by Biomer (Krailling, Germany), on a customized pilot melt-spinning plant originally built by Fourné Polymertechnik (Alfter-Impekoven, Germany). Fiber no. 974 (fiber label given by Empa, St. Gallen, Switzerland) was melt-spun from a pelletized P3HB compound (Mw = 0.5 MDa), whereas raw P3HB powder (Mw = 1.6 MDa), mixed with 20 wt% plasticizer (tri-nbutyl citrate (TBC)), was used to melt-spin fiber no. 1108. The P3HB pellets, used for fiber 974, contained a nucleating agent (boron nitride (BN)), 20 wt% TBC and various other processing aids, including low molecular weight poly-ε-caprolactone (PCL). The fiber diameters are about 90 μm for both fibers. Fiber 974 was melt-spun with a draw ratio (DR) of 7.0, and fiber 1108 with DR = 6.0. More detailed information about materials, properties and melt-spinning parameters can be found in our previous publications [8,9,11]. We label fiber 974 with (I) and fiber 1108 with (II) in the remainder of this article. We have studied these two fibers with synchrotron WAXD and ATR-FTIR as a continuation of our previous work [8,9,11], in order to investigate if the mesophase dissolution and reversibility is present in low-stress annealed fibers, melt-spun from different P3HB compounds.

2.2. Stress-annealing of P3HB fibers

The stress-annealing of aged (eight years at 23 °C) P3HB fibers was carried out by attaching different weights (1 g, 5 g, 10 g, 16 g, 20 g, 25 g) to the fibers, corresponding to applied stresses of 1.6, 8.0, 16.0, 25.6, 32.0 and 40.0 MPa. The annealing was performed in a furnace with hot air circulation at different temperatures (80, 100, 115, 130 °C) for 60 min. Above 100 and 115 °C, respectively, fibers (I) and (II) were only annealed at low stress (1.6 MPa). Applying higher stresses at elevated temperatures resulted in fiber breakage within a few minutes. The length of each monofilament was measured at room temperature, with an applied weight of 1 g (pre-stress of 1.6 MPa), before and after annealing, in order to determine the change in filament diameter and thus the linear mass density.

Table 1
Annealing conditions of stress-annealed fiber samples, as well as fineness and diameters.

Fiber label	Annealing stress (MPa)	Annealing weight	Annealing temperature (°C)	Fineness (tex = mg/m)	Diameter[a] (μm)
(I)		–	–	Original: 7.4	90
	1.6	1 g	80	9.5	100
	8.0	5 g	80	8.1	93
	16.0	10 g	80	7.3	88
	32.0	20 g	80	6.9	85
	40.0	25 g	80	6.5	83
	1.6	1 g	100	10.0	103
	16.0	10 g	100	7.2	87
	25.6	16 g	100	6.5	83
	32.0	20 g	100	6.2	81
	1.6	1 g	115	10.5	106
	1.6	1 g	130	10.9	107
(II)	–	–	–	Original: 7.5	90
	1.6	1 g	80	9.1	98
	8.0	5 g	80	8.2	94
	16.0	10 g	80	7.7	91
	32.0	20 g	80	7.4	89
	40.0	25 g	80	7.1	87
	1.6	1 g	100	9.6	101
	16.0	10 g	100	7.6	90
	25.6	16 g	100	7.0	86
	32.0	20 g	100	6.3	82
	40.0	25 g	100	6.2	81
	1.6	1 g	115	10.1	104
	8.0	5 g	115	9.1	98
	16.0	10 g	115	7.9	92
	25.6	16 g	115	7.0	86
	1.6	1 g	130	10.5	106

[a] Diameters are calculated from the fineness, assuming a circular fiber and a density of P3HB of 1.2 g/cm^3 [11].

The annealing conditions, as well as fineness and diameter of all analyzed stress-annealed fiber samples, are summarized in Table 1.

2.3. Characterization

2.3.1. In-situ wide-angle x-ray diffraction at the synchrotron

In-situ WAXD measurements were performed at the cSAXS beamline at the Swiss Light Source synchrotron of the Paul Scherrer Institute in Switzerland. Differently annealed monofilaments have been mounted on a sample holder (horizontally) and WAXD patterns were measured at the center of the fibers with 5 s exposures using a Pilatus 2 M detector [19]. The sample to detector distance was 31.9 cm. The x-ray beam was focused with mirrors to a spot size of about 10 μm (perpendicular to fiber axis) and its energy was set to 11.792 keV. The resulting WAXD patterns were rotated by 90°. Horizontal lines, arising from module gaps, have been filled with symmetrized patterns, and the right side of the image was taken to be the same as the left. However, vertical lines, arising from module gaps, could not be properly filled, since the direct beam was horizontally located in the center of a detector module. All WAXD patterns have been normalized by the fiber diameters in order to account for the changes in the illuminated scattering volume. Since the beam size perpendicular to the fiber axis (~10 μm) was smaller than the fiber diameter, the illuminated cylindrical scattering volume in the center of the fiber is approximately proportional to the fiber diameter. Equatorial profiles have been extracted by converting the pixel positions to polar coordinates and radially integrating the pixels that are located within the equatorial sector (opening angle is 20°).

The cyclic drawing at room temperature was performed on filaments annealed at low stress (1.6 MPa), using a TS 600 tensile stage (Anton Paar GmbH, Austria) with a 5 N load cell. A pre-annealed single filament was glued on top of supports and held by tensile stage grips. The single filament was elongated with a rate of 0.5 mm/min to about 50% elongation or more, followed by relaxation, while exposing the filament to the synchrotron x-ray beam every 30 s for 0.5 s. Typically, two or more cycles have been measured before drawing the fiber to the breaking point. Again, a Pilatus 2 M detector was used to capture the WAXD patterns, using a sample to detector distance of 29.35 cm. The x-ray beam was focused with mirrors to a spot size of about 50 μm perpendicular to the fiber axis, and to a spot size of about 75 μm along the fiber axis.

2.3.2. Polarized attenuated total reflection fourier transform infrared spectroscopy

Polarized ATR-FTIR spectra have been recorded from differently stress-annealed P3HB fibers with a Bruker Tensor 27 FTIR spectrometer (Bruker Optics, Ettlingen, Germany), using a single reflection attenuated total reflectance (GladiATR™) accessory from Pike Technologies (Fitchburg, Wisconsin, United States). The FTIR spectrometer uses a mid-infrared (MIR) Globar source and a narrow-band mercury cadmium telluride (MCT) detector. The ATR accessory is equipped with a monolithic diamond ATR crystal but does not have the option to add polarizers. Thus, we have custom-built a mount for the polarizer and have attached it to the entry opening of the GladiATR™ accessory [20]. The infrared light was guided through a linear germanium polarizer from Pike Technologies (Fitchburg, Wisconsin, United States), followed by guiding it through the optics chamber of the GladiATR™ accessory to the fiber sample surface, with an angle of incidence of $\theta = 45°$. The depth of penetration, Δz, of the infrared light into the polymer material is typically below 5 μm, as the following equation shows [21]:

$$\Delta z = \frac{\lambda}{2\pi n_1 \left(sin^2\theta - (n_2/n_1)^2 \right)^{0.5}} \quad (1)$$

where $n_1 \sim 2.4$ and $n_2 \sim 1.47$ [22] are the refractive indices (dispersion is neglected) of the ATR crystal and the investigated polymer, respectively, and λ is the wavelength.

A reproducible contact pressure between the ATR crystal and the fiber was ensured by manipulating the pressure clamp of the ATR system in the exact same way for each measurement. The manual linear polarizer was rotated to either 45° or 135° in order to achieve *p* or *s* polarized light at the fiber surface, respectively (Fig. 1).

For static ATR-FTIR measurements, where no tensile stress was applied, a special fiber holder was custom-built and attached to the GladiATR tabletop, in order to reproducibly orient the fibers in the direction perpendicular to the path of the infrared light [20]. Additionally, a second sample holder was 3D printed [20], in order to measure ATR-FTIR spectra of fibers that have been stretched or released to specific elongations during cyclic tensile testing. The fibers were glued onto the holder's movable slide with Scotch Gel Universal adhesive (3 M GmbH, Switzerland). The initial distance between the two fixing points, where the glue was applied, was chosen to be 2 cm for all fiber samples. During the measurement, the movable slide of the holder was moved by 4 mm increments (20%, 40%, 60% elongation), followed by a measurement of an ATR-FTIR spectra in *s*-polarization. After reaching the maximum elongation (60%), the holder was pushed back to the previous strain values (40%, 20%) without slacking of the fiber samples, and the ATR-FTIR measurements were repeated.

Absorbance spectra, spanning wavenumbers between 4000 and 600 cm^{-1}, were collected with a spectral resolution of 2 cm^{-1}. For each spectrum, a total of 32 scans have been acquired and averaged. To minimize differences between spectra, the spectra were cut in the range of 4000 to 750 cm^{-1}, and the baselines were subsequently subtracted by using a concave Rubber band algorithm with 10 iterations using OPUS™ software (Version 8.5, Bruker AXS, Karlsruhe, Germany). Additional data analysis, such as normalization and plotting, was performed with specifically developed Python codes.

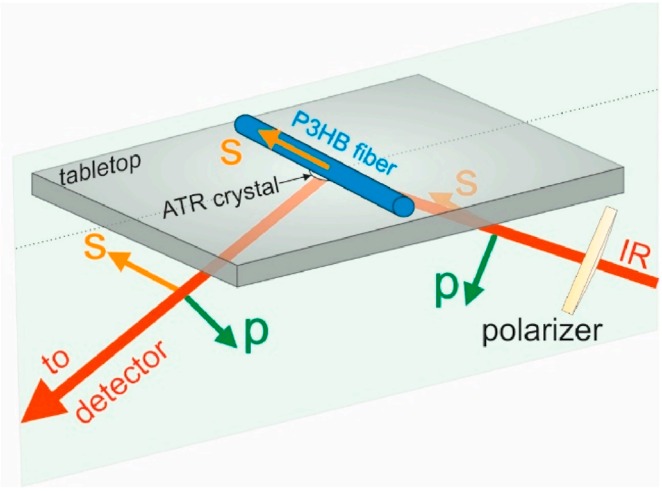

Fig. 1. Polarized ATR-FTIR measurement of P3HB monofilaments.

3. Results and discussion

3.1. Synchrotron WAXD analysis of stress-annealed P3HB fibers

3.1.1. Absence of mesophase off-axis reflections in WAXD patterns of P3HB fibers

As mentioned in the introduction section, two broad equatorial reflections and off-axis reflections above the 1st layer line [17,18] have been observed for highly stretched P3HB films, and authors have suggested that these reflections arise from a hexagonal β-crystalline phase. With laboratory X-ray sources [8,9], we have detected no off-axis reflections above the 1st layer line in original and stress-annealed P3HB fibers, which led us to the conclusion that the phase is a non-crystalline mesophase. In order to confirm this previous finding, we have measured WAXD patterns with a synchrotron X-ray beam. A vertically symmetrized WAXD pattern of the original fiber (I) is shown in Fig. 2. The highly oriented crystalline α-phase with helical P3HB molecules (Fig. 2a) leads to sharp reflections in the WAXD pattern (Fig. 2b). A close-up of the region around the (110) equatorial reflection and the first layer line is shown in (Fig. 2c). Fig. 3 shows the same WAXD close-ups for differently stress-annealed P3HB fibers (I) at 80 and 100 °C. To highlight the weaker intensities, the WAXD patterns are shown on a logarithmic intensity scale.

No reflections above the 1st layer line have been observed, neither in the WAXD patterns of the original fiber (Fig. 2c), nor in the patterns of high-stress annealed fibers (Fig. 3). This finding agrees with our previously published work, that is based on WAXD patterns measured with a laboratory X-ray source [8,9,11]. Note that other authors have also published WAXD patterns, where no off-axis reflections are visible above the 1st layer line in P3HB or P3HBV fibers [16,23,24]. Only broad equatorial non-crystalline mesophase peaks (P_{nc}) are observed for the original (Fig. 2c) and stress annealed fibers (I) (Fig. 3). The same is observed for stress-annealed fibers (II) [20].

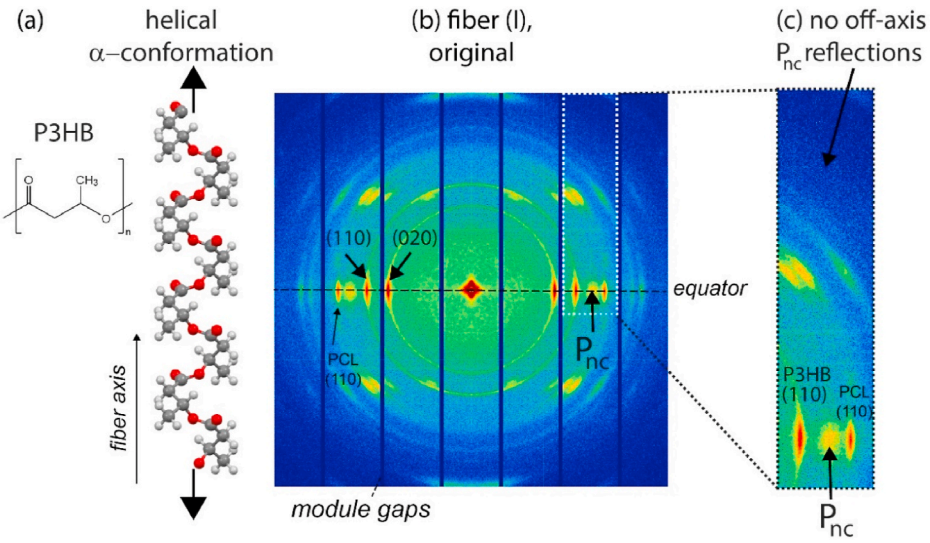

Fig. 2. (a) Chemical structure of P3HB and a molecular model of the helical α-conformation [10], which we have illustrated using the Mercury software [25]. (b) The measured, symmetrized WAXD pattern of the original fiber (I). (c) A close-up of the equatorial and first layer line region, including the equatorial non-crystalline mesophase (P_{nc}) peak.

3.1.2. *Mesophase content dependency on annealing conditions*

In Fig. 3, for fibers annealed at low stress (1.6 MPa), the mesophase seems to disappear, and its peak intensity increases with the annealing stress. Interestingly, the mesophase peak is already visible for low stress values (16 MPa) at low temperature (80 °C), which is not the case for higher temperatures, where a stress of 32 MPa is needed for the mesophase to appear (Fig. 3). To better compare the mesophase peak intensities of differently annealed P3HB fibers, we have extracted equatorial profiles from the WAXD patterns, through radial integration of an equatorial sector with an azimuthal angle of 20°. Fig. 4a and b shows the extracted equatorial profiles from WAXD patterns for stress-annealed fibers (I) at 80 °C and 100 °C, respectively. The measured profiles of fiber (I) for 130 °C, and all profiles for stress-annealed fibers (II), are shown in the data in brief article [20]. Fig. 4c and d shows the evolution of mesophase and of (110) peak areas, respectively, as a function of applied annealing stress at annealing temperatures 80 °C, 100 °C and 130 °C. For fibers annealed at low-stress, the mesophase practically disappeared compared to the original fiber, since the stretched chains from the mesophase recoil and contribute to the α-crystals. Overall, the mesophase content is clearly increasing with increasing annealing stress, compared to the fiber annealed at low-stress (Fig. 4c). Due to the high stress, molecular chains (tie molecules in-between crystals, or molecules in the amorphous phase) become more stretched and thus contribute to the mesophase. Furthermore, for high annealing stress, the mesophase intensity is slightly higher than for the original fiber, which explains the previously found higher tensile strength of high-stress annealed fibers [8]. For fibers annealed at low stress (1.6 MPa), the mesophase almost completely disappeared. Note that for the lowest temperature, 80 °C, less mesophase was lost than for high annealing temperatures. This finding suggests that higher temperatures are needed to completely dissolve the mesophase. For a given annealing stress, the transformation from α-crystals into the mesophase becomes more difficult with increasing temperature, since the growth of the crystals at higher temperatures outplays the mesophase formation. At elevated temperatures, the chains of amorphous phase and mesophase gain sufficient mobility to recoil to helical α-conformations, and thus they contribute to α-crystals. For all annealing conditions, the annealing temperatures lay above or close to the cold-crystallization temperature. In consequence, the α-crystals have grown, which is reflected by the overall higher (110) peak areas (Fig. 4d) and smaller (110) peak widths of the annealed samples, compared to the ones of the original fiber. The growth of α-crystals at the expense of the mesophase

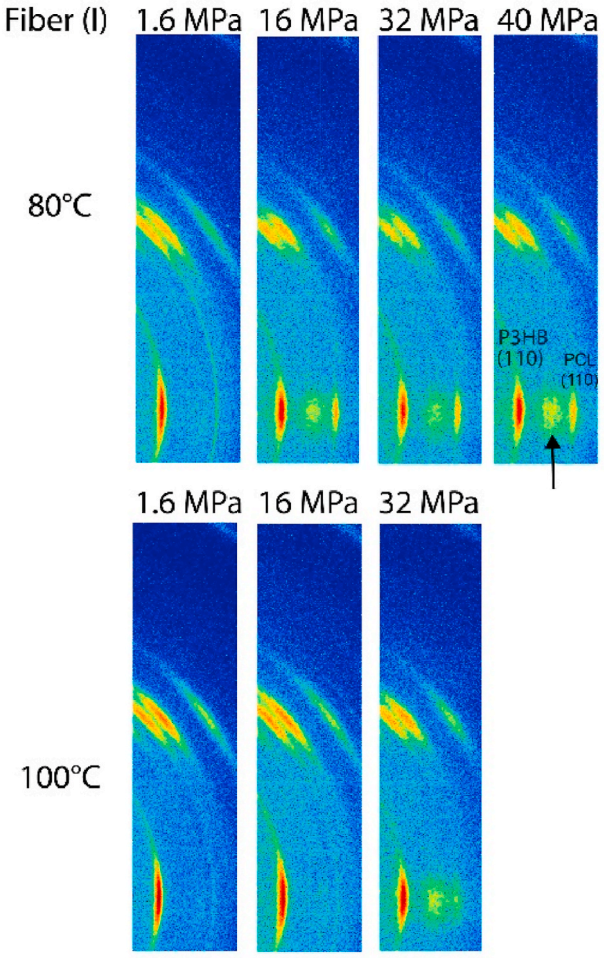

Fig. 3. Close-ups of WAXD patterns measured at the synchrotron with 5s exposures. Stress-annealed fiber (I) at 80 °C (top row) and at 100 °C (bottom row) with 1.6, 16, 32 MPa and 40 MPa, respectively. Note that at 100 °C, it was not possible to anneal fibers with applied stresses of 40 MPa, since they broke during the annealing procedure.

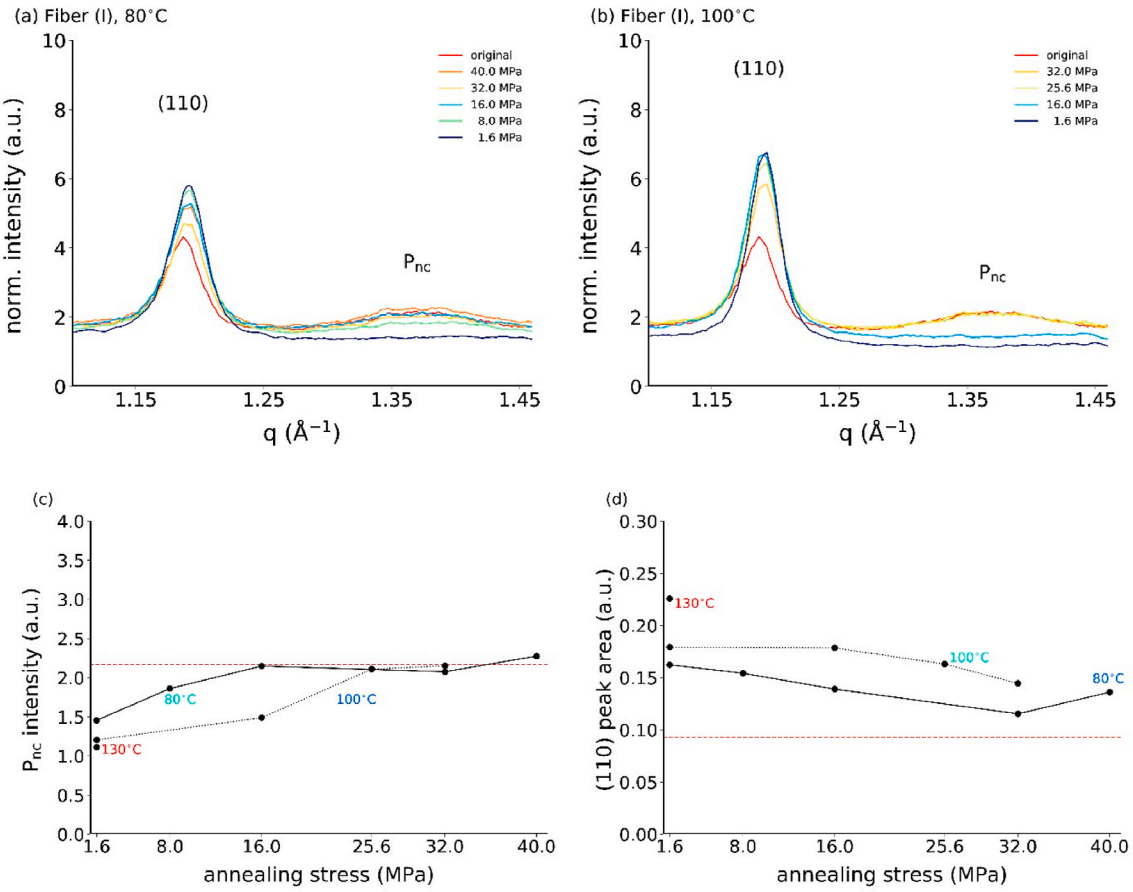

Fig. 4. Equatorial profiles for stress-annealed fiber (I) at (a) 80 °C and (b) 100 °C. (c) Mesophase peak intensity and (d) peak area of (110) crystalline planes as a function of the annealing stress. The dashed horizontal red lines in (c) and (d) are the reference values of the original fiber (I). (For interpretation of the references to colour in this figure legend, the reader is referred to the Web version of this article.)

results in a lower tensile strength and a larger elongation at break of the fibers [8]. For a given annealing stress, the crystallinity increases with augmenting temperature due to the enhanced mobility of the macromolecules. A similar behavior was observed for fiber (II), with the following differences: (a) it was possible to apply higher stresses at higher temperatures (e.g. 115 °C, 25.6 MPa), which may be a result of the lower initial draw ratio of fiber (II) compared to fiber (I), but could also be influenced by other factors like molecular weight or nucleating agents in the material, (b) the mesophase increased rather linearly with increasing annealing stress [20]. We suspect that the lower initial draw ratio of fiber (II) leads to less stretched chains in the original fiber, and thus, that the mesophase can grow up to higher stresses in fiber (II) than in fiber (I). Note that other factors like molecular weight or additives could also have an effect on the mesophase formation. In fiber (I), a saturation point of the mesophase formation is already reached at 16 MPa. Thermal properties and calculated average crystallinities from differential scanning calorimetry (DSC) measurements of stress-annealed P3HB fibers are also shown in the data in brief article [20]. Crystallinity values, calculated from the P3HB melting peak in the DSC first heating thermograms, confirm that for a given annealing stress the crystallinity increases with increasing annealing temperature. DSC reveals that fiber (II) has a ~10% higher crystallinity than fiber (I). Most-likely the additives in fiber (I) hinder the crystallization of P3HB.

3.2. *In-situ synchrotron WAXD during cyclic drawing of P3HB fibers annealed at low stress*

In-situ synchrotron WAXD measurements served to answer the question, if the formation/dissolution of the mesophase in fibers annealed at low stress during cyclic tensile drawing is reversible, and how this depends on the annealing temperature. The left-side of Fig. 5 shows sequences of equatorial profiles from WAXD patterns of fibers (I, II) annealed at low stress (1.6 MPa at 80 °C and 115 °C), which have been measured during cyclic tensile drawing. The profiles have been normalized to the initial (020) peak intensity at 0% strain. Corresponding stress-strain curves are shown on the right-hand side of Fig. 5. The points indicate the positions where WAXD patterns have been measured, and the numbers correspond to the image number axis of the equatorial profiles. The images, resulting from the positions where the x-ray beam hit the fiber sample, are consecutively numbered. Sometimes the x-ray beam missed the fiber during drawing or release of the filament, thus those data points have been skipped. In each cycle, the filament has been realigned at maximum load. Fig. 5 shows that the formation of the mesophase, in fibers annealed at low stress, is highly

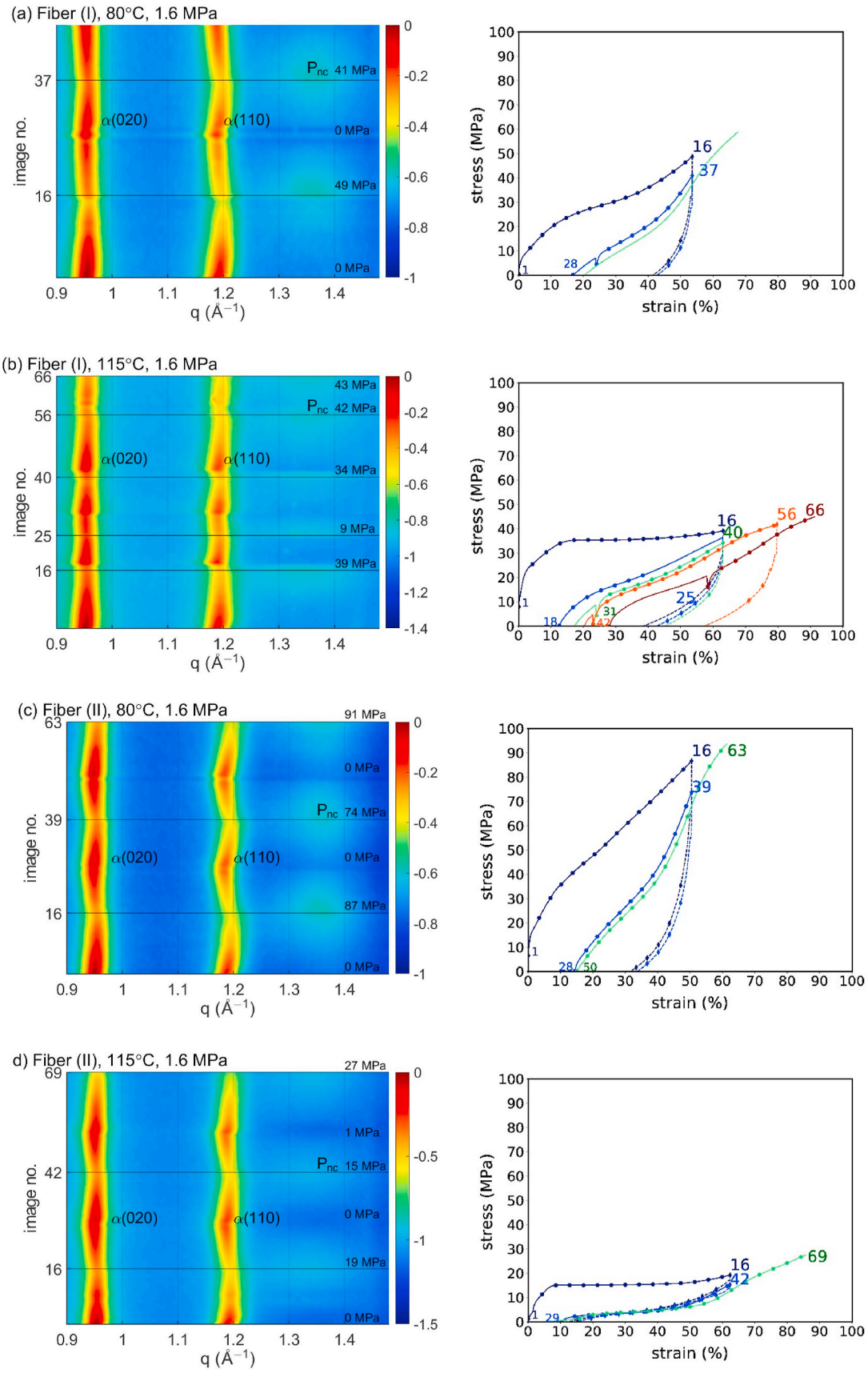

Fig. 5. Left: Sequences of equatorial profiles during cyclic tensile drawing of fibers annealed at low stress (1.6 MPa): fiber (I) annealed at (a) 80 °C and at (b) 115 °C, as well as fiber (II) annealed at (c) 80 °C and (d) 115 °C. The intensity is shown on a logarithmic scale. Right: Corresponding stress-strain curves. The points indicate the positions where WAXD images were analyzed, and the numbers indicate the respective image numbers.

reversible for both fibers, and that the growth of the mesophase always occurs at the expense of the α-crystals. Upon drawing, the chains are pulled out of the crystalline α-phase and become elongated and stretched, forming the mesophase. When the fiber is released, the mesophase chains partially recoil to the helical conformation and contribute again to the α-phase reflections. Such cycles have been repeated several times until fiber breakage. The mesophase peaks at about 50% strain are higher in intensity and sharper for the fibers annealed at 80 °C, compared to those annealed at 115 °C. This finding correlates with a higher tensile strength of the former fibers. The mesophase at 50% strain is higher in intensity for the annealed fiber at 80 °C, since the initial mesophase content at 0% strain is already higher. The sharpness of the mesophase peak also suggests that the chains that are pulled out of the α-crystals, and that are being stretched, have a well-defined lateral spacing.

3.3. Polarized ATR-FTIR analysis of stress-annealed P3HB fibers

Polarized ATR-FTIR measurements on stress-annealed fibers served to determine how the mesophase content depends on the annealing conditions (temperature and stress). The goal was to correlate differences in polarized ATR-FTIR spectra of stress-annealed fibers with the structural differences seen in WAXD patterns. Note that the ATR-FTIR spectra reveal structural information about the fiber surfaces, and the WAXD data reveal information about the average molecular structure of the fibers.

We have performed polarized ATR-FTIR measurements on original and stress-annealed P3HB fibers. As mentioned in the experimental section, the electric field vector of the *s*-polarized incoming infrared light points along the fiber axis (Fig. 1). Maximum IR absorption occurs when the electric field vector and the transition dipole moment are

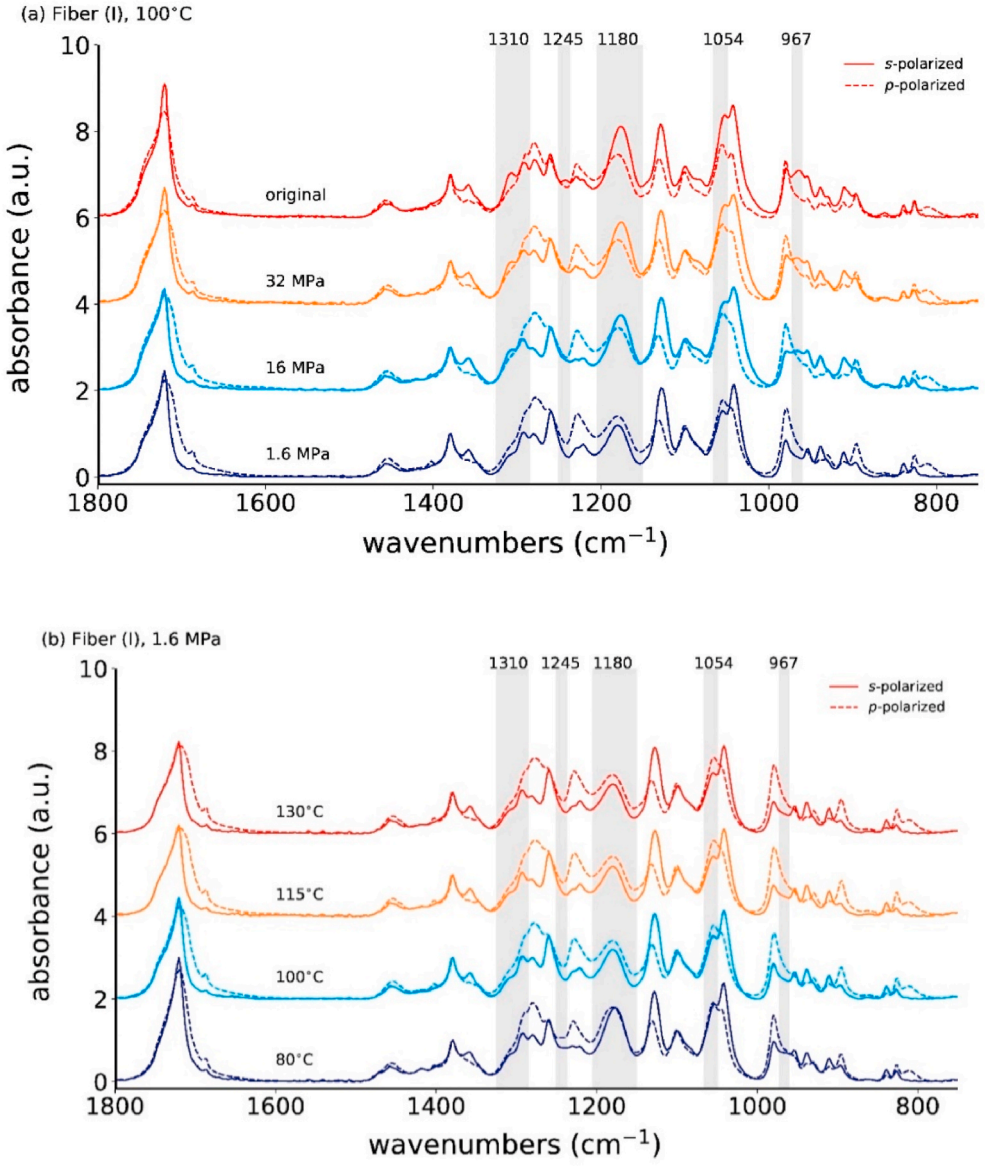

Fig. 6. Polarized ATR-FTIR spectra for (a) the original and stress-annealed fiber (I) at 100 °C with different applied stresses and (b) for the fibers (I) annealed at low stress (1.6 MPa) at different temperatures. The curves are offset for better visibility.

Table 2
Assignments of analyzed infrared bands to vibrations in P3HB.

Wavenumber (cm^{-1})	Assignment	Reference
1740	νC = O (amorphous)	[29]
1724	νC = O (α-crystal)	[29]
1454	δCH_2, $\delta_{as}CH_3$ (α-crystal)	[29]
1380	$\delta_s CH_3$ (α-crystal)	[29,30,32]
1308	amorphous	[29]
1310(s)	mesophase ("β-conf.")	[17]
1310(s)*	mesophase	
1290	helical conf. (α-crystal)	[29]
1291(s),	mesophase ("β-conf.")	[17]
1291(s)*	mesophase	
1280	wCH_2 (α-crystal)	[29]
1264	helical conf. (α-crystal)	[29]
1245(s)*	mesophase	
1230	helical conf. (α-crystal)	[29]
1185	νasC-O-C (amorphous)	[29]
1185(s)	mesophase ("β-conf.")	[17]
1080(s)*	mesophase	
1133	νsC-O-C	[29]
1082(s)	mesophase ("β-conf.")	
1085(s)*	mesophase	[17]
1058	νC–CH_3	
1054(s)*	mesophase	[29]
980	rCH3, νC–C (α-crystal)	[29]
970(s), 976(s)*	mesophase ("β-conf.")	[17]
954 (s)	helical conf. (α-crystal)	[17]
857(s, p)	mesophase ("β-conf.")	[17]
446(s)	mesophase ("β-conf.")	[17]

(*s*) s-polarized; parallel to drawing axis, (*p*)-polarized; perpendicular to drawing axis, *found peak position in this publication.

parallel to each other [26]. Thus, changes in the spectra acquired with *s*-polarized infrared light are related to vibrational modes, where the transition dipole moments are aligned parallel to the fiber axis.

The *s*- and *p*-polarized spectra for the original and annealed fiber (I) at 100 °C, with applied stresses ranging from 1.6 MPa to 32 MPa, are shown in Fig. 6a. Fig. 6b shows the spectra for a constant applied stress of 1.6 MPa, but different annealing temperatures. The curves have been offset for better visibility. All ATR-FTIR spectra have been normalized with respect to the peak at 1380 cm^{-1}, which corresponds to the symmetric bending mode of the CH_3 functional group. The shaded regions in Fig. 6 highlight the IR bands, which are attributed to vibrations of functional groups of stretched chains in the mesophase.

Assignments of IR bands to vibrational modes of functional groups of P3HB have been previously reported [27–30], and the most-relevant ones are summarized in Table 2. The bands that have been reported to be sensitive to changes in crystallinity are: 1724, 1454, 1280, 1230 and 1185 cm^{-1} [27–32], where the latter band strongly decreases with increasing crystallinity, while the others typically increase.

Recently, polarized ATR-FTIR has been performed on stretched P3HB films in order to investigate the stress-induced mesophase [17]. Some IR bands have been attributed to the zigzag conformation of stretched chains, which are also summarized in Table 2. These bands, in *s*-polarization (electric field vector points along the drawing axis), have been reported to increase in absorbance with increasing tensile strain. The mesophase chains are expected to be highly oriented along the fiber axis. Thus, differences in the mesophase content are expected to be seen in the *s*-polarized spectra. Overplots of *s*-polarized ATR-FTIR spectra for different applied annealing stresses at constant annealing temperature (100 °C) are shown in Fig. 7a, and overplots for different annealing temperatures, but constant annealing stress (1.6 MPa), are shown in Fig. 7b.

We have previously shown with WAXD, that the mesophase content is high in the original fiber as well as in the fibers annealed at high stress. Therefore, the *s*-polarized ATR-FTIR spectra for the original and high-stress annealed samples (32 MPa and 16 MPa) are very similar in Fig. 7a, and resemble the previously published spectrum of highly stretched P3HB films [17]. Interestingly, some bands in the *s*-polarized spectrum of the fiber annealed at low stress (1.6 MPa) are absent or have a significantly lower absorbance. These IR bands (1310 cm^{-1}, 1291 cm^{-1}, 1245 cm^{-1}, 1180 cm^{-1}, 1085 cm^{-1}, 1054 cm^{-1}, 967 cm^{-1}) can thus be attributed to the mesophase and are indicated with vertical dotted lines in Fig. 7a and b. Note that most of these band positions are identical or close to the previously published positions for mesophases in P3HB films [17]. The newly identified IR bands, which are also sensitive to the mesophase, are located at 1245 cm^{-1} and 1054 cm^{-1}. Fig. 7b shows that there is a residual mesophase content in the fiber annealed at 80 °C under low stress (1.6 MPa) (higher absorbances at 1245, 1180, 1054, 967 cm^{-1}), whereas the mesophase in the fibers annealed with low stress at higher temperatures is practically gone. We have measured *s*-polarized ATR-FTIR on all stress-annealed fibers and have analyzed the dependence of the mesophase IR bands on the annealing stress [20]. Fig. 8 shows the absorbance of the 967 cm^{-1} IR band as a function of the annealing stress. The dependences of other mesophase IR bands for fiber (I) and (II) are shown in the data in brief article [20]. The dependence of the mesophase IR band 967 cm^{-1} in Fig. 8 on the annealing stress strongly resembles the one of the WAXD equatorial mesophase peak in Fig. 4c. Due to the differences in the measuring techniques, e.g. ATR-FTIR probes the fiber surface, and WAXD probes the entire fiber cross-section, slight differences in the progression of the curves can be observed. This correlation is also present for the other identified mesophase IR bands [20]. Thus, the identified IR bands are definitely correlated with the mesophase.

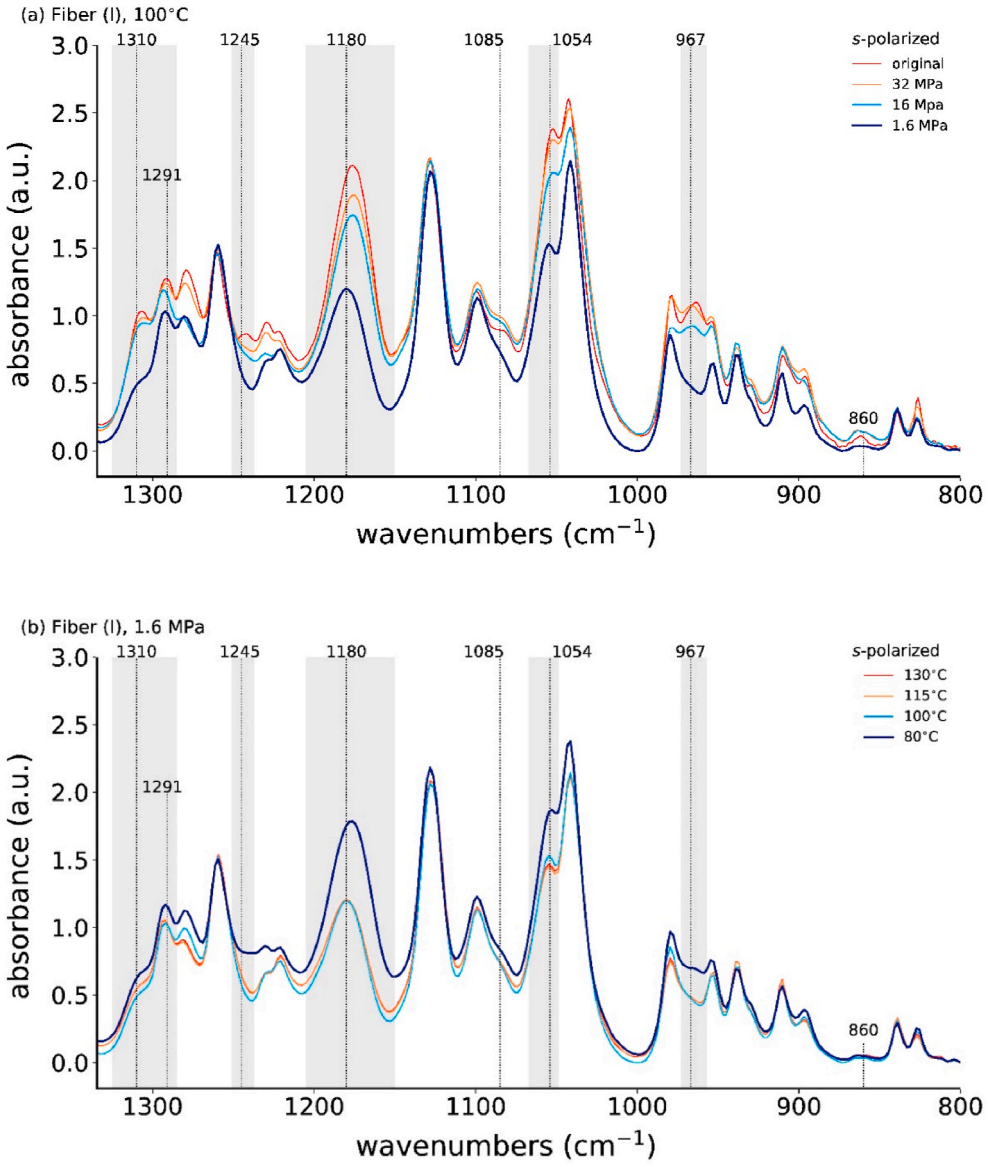

Fig. 7. Overplots of ATR-FTIR spectra with s-polarization for the original and stress-annealed fiber at (a) 100 °C with different applied stresses and with (b) a fixed applied stress (1.6 MPa) but varying annealing temperatures.

3.4. In-situ polarized ATR-FTIR under cyclic drawing of P3HB fibers annealed at low stress

Cyclic polarized ATR-FTIR measurements have been carried out to support the findings regarding reversibility of formation/dissolution of the mesophase, gained from in-situ synchrotron WAXD measurements (section 3.2). For this purpose, fiber samples have been annealed at 80, 115 and 130 °C with an applied stress of 1.6 MPa. This study was performed in order to determine how the absorbances of the IR bands correlate with the previously observed reversible structural changes.

As described in the experimental section, the fiber samples have been stretched to elongations 20, 40 and 60%, followed by measurements of *s*-polarized ATR-FTIR spectra. After the highest stretching, the fiber samples were allowed to relax back to elongations of 40 and 20%. Below an elongation of 20%, the fibers started to bend. Fig. 9a shows the cyclic ATR-FTIR results (*s*-polarized) of the fiber sample, which has been previously annealed at 115 °C with 1.6 MPa. All absorbances of IR bands, which have been identified to be related to the mesophase (section 3.3), are increasing with increasing stress and decrease upon relaxation (Fig. 9b). These findings are in agreement with WAXD results, where a cyclic increase and decrease in the mesophase content has been observed (section 3.2). Thus, we conclude that the mesophase formation/dissolution is highly reversible. Another observation shows that the peak at 967 cm^{-1} shifts to about 964 cm^{-1} when the fiber is stretched to 60% elongation. This suggests that bond lengths increase upon stretching, as expected. We also observe that additional IR bands (928, 911, 897, 860, 827 cm^{-1}) show a highly reversible increase and decrease in absorbance. The peak at 911 cm^{-1} becomes rather broad and intense

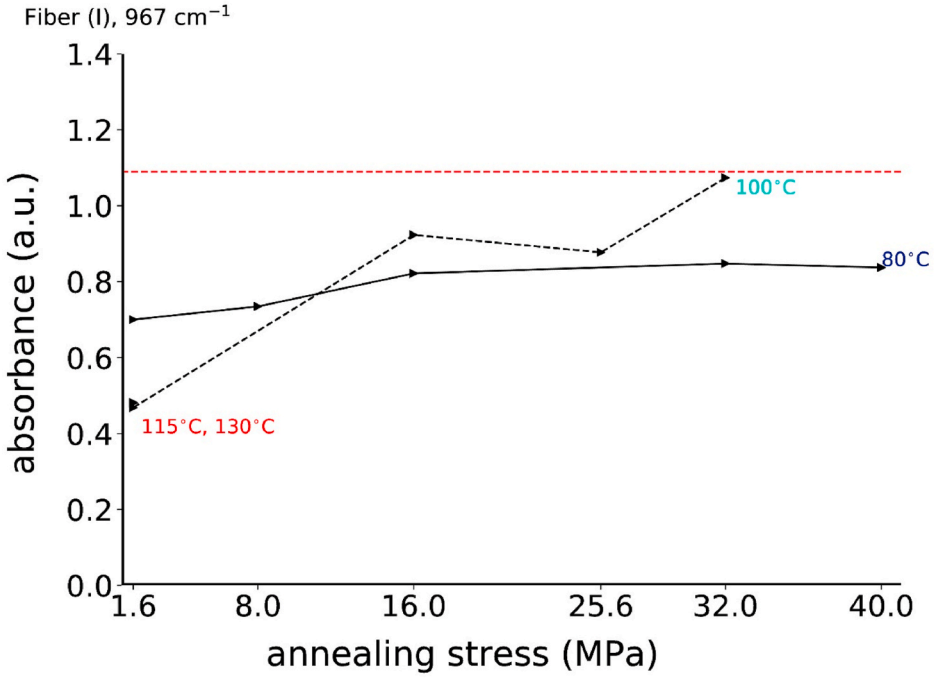

Fig. 8. Absorbance of the 967 cm^{-1} IR band as a function of the annealing stress at 80, 100, 115 and 130 °C. The dashed horizontal red line is the reference value of the original fiber (I). (For interpretation of the references to colour in this figure legend, the reader is referred to the Web version of this article.)

for large stretch values, and thus, the double peak at 911, 897 cm^{-1} merges into one, to form a fairly broad peak.

Fig. 10 compares the absorbances of the mesophase IR band 967 cm^{-1} of the fibers annealed at low stress (80, 115, 130 °C with 1.6 MPa) as a function of the stretching sequence. A higher mesophase content is observed for the stretched fiber, which has been annealed with low stress at 80 °C. This finding is in agreement with the WAXD results in section 3.1.2.

4. Conclusion

Synchrotron WAXD and polarized ATR-FTIR spectroscopy was used to A) analyze structural modifications to P3HB fibers due to stress-annealing and to B) study the reversibility behavior of the mesophase formation/dissolution during cyclic drawing of annealed P3HB fibers at low stress.

A) WAXD patterns and *s*-polarized ATR-FTIR spectra have shown similar dependencies of the mesophase content on the annealing conditions. In the WAXD patterns, equatorial peaks that arise from the mesophase, increase in intensity with increasing annealing stress. For fibers annealed at low stress, the mesophase almost disappears. Fibers that have been annealed at 80 °C under low stress have shown a higher remaining mesophase content than fibers annealed at high-temperature (>80 °C). In consequence, at high temperatures and low annealing stresses (e.g., 115 °C and 1.6 MPa), the macromolecules have a higher mobility, and thus stretched macromolecules from the mesophase recoil into the helical α-conformation. A higher mesophase content than the original fibers can be achieved for annealing conditions with high stress (40 MPa) (Fig. 4c). In *s*-polarized (electric field vector along the fiber axis) ATR-FTIR spectra, specific IR bands have been identified to arise from the P3HB mesophase (Table 2). The absorbances of these bands also increase with increasing annealing stress. Polarized ATR-FTIR spectroscopy has been demonstrated to be an ideal tool to study mesophases in polymer fibers, and should thus also be applied to other oriented polymeric materials in the future.

B) In annealed fibers at low stress, the mesophase content has practically disappeared. We have therefore studied such fibers during cyclic tensile drawing with in-situ WAXD and polarized ATR-FTIR spectroscopy. It was shown that the mesophase can be recovered through tensile drawing, and that the formation/dissolution of this mesophase is highly reversible. This finding, combined with the fact that no off-axis reflections have been found above the 1st layer line in WAXD patterns of original and high-stress annealed fibers, suggests that the mesophase is non-crystalline in nature, and that it is made of conformationally disordered stretched chains in-between α-crystals.

Funding sources

There are no funding sources to declare.

Data availability

Raw data is available to download from https://doi.org/10.17632/cpdyrdfx9y.1.

CRediT authorship contribution statement

E. Perret: Software, Formal analysis, Investigation, Data curation, Writing – original draft, Visualization. **K. Sharma:** Data curation, Writing – review & editing. **S. Tritsch:** Data curation. **R. Hufenus:** Supervision, Project administration, Writing – review & editing.

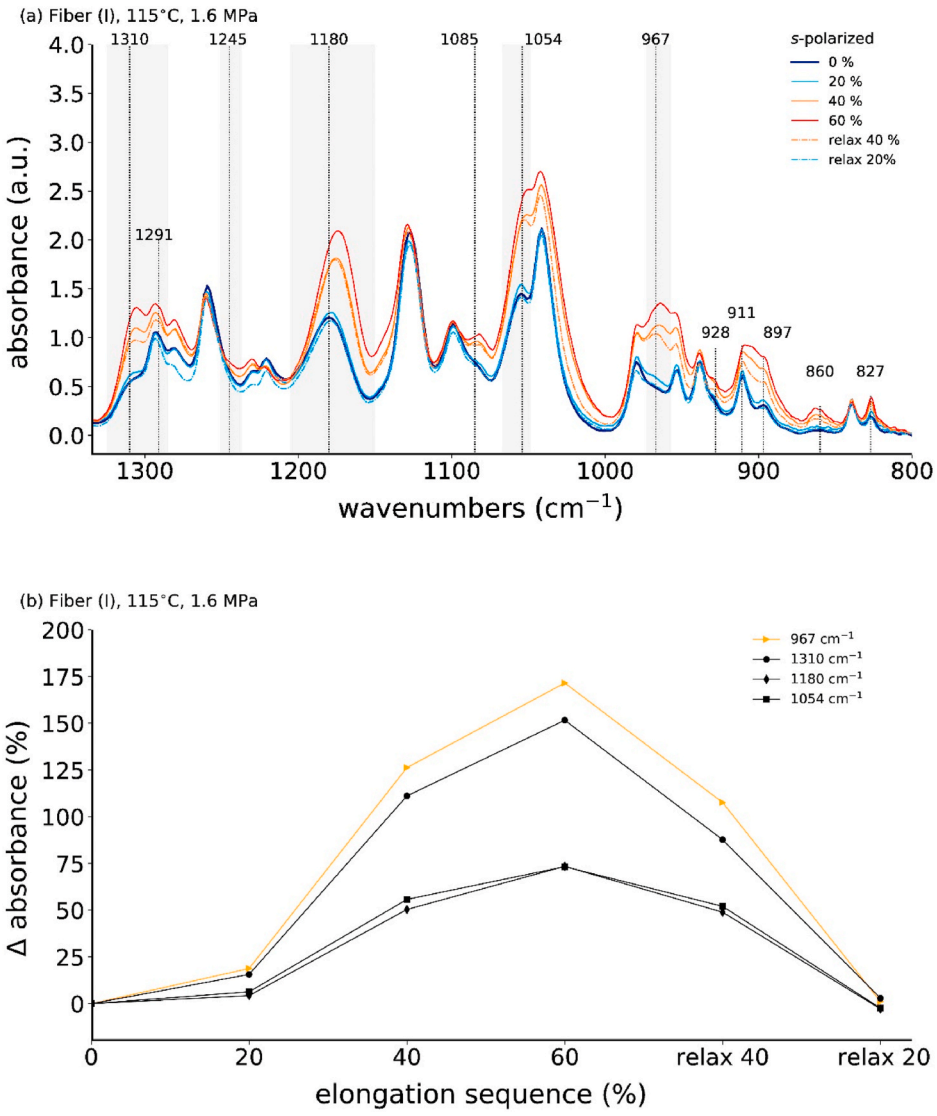

Fig. 9. (a) Normalized in-situ ATR-FTIR spectra with *s*-polarization during cyclic tensile drawing (one cycle) of P3HB fiber (I), which has been previously annealed at 115 °C with 1.6 MPa and (b) corresponding percentage change in absorbance (with respect to 0% elongation) of mesophase IR bands as a function of elongation sequence.

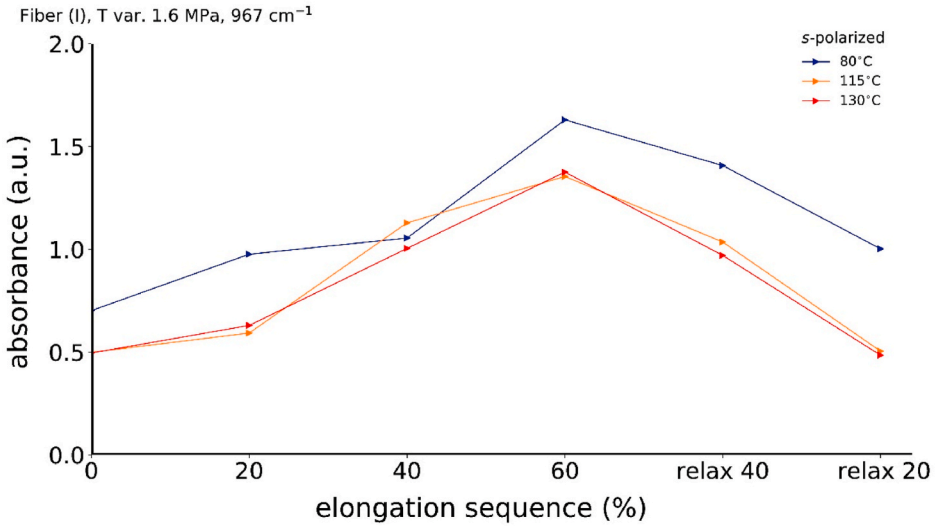

Fig. 10. Absorbance of the 967 cm^{-1} IR band as a function of the elongation sequence for samples that have been annealed at 80, 115 and 130 °C with 1.6 MPa.

Declaration of competing interest

The authors declare that they have no known competing financial interests or personal relationships that could have appeared to influence the work reported in this paper.

Acknowledgments

Authors would like to thank Markus Hilber for helping with the operation of the annealing furnace and 3D printing of sample holders. We also thank Benno Wüst for operating the melt-spinning plant. The authors thank Andreas Menzel from the cSAXS beamline at the Swiss Light Source, PSI, Switzerland for his support during the beamtime.

References

[1] M. Dake, Biodegradable polymers: renewable nature, life cycle, and applications, in: V.C. Kalia (Ed.), Microbial Factories: Biodiversity, Biopolymers, Bioactive Molecules, ume 2, Springer India, New Delhi, 2015, pp. 29–56.
[2] M.P. Fernández-Ronco, et al., Tuning poly(3-hydroxybutyrate) (P3HB) properties by tailored segmented biocopolymers, ACS Sustain. Chem. Eng. 5 (11) (2017) 11060–11068.
[3] B. Laycock, et al., The chemomechanical properties of microbial polyhydroxyalkanoates, Prog. Polym. Sci. 38 (3–4) (2013) 536–583.
[4] Y.K. Leong, et al., Current trends in polyhydroxyalkanoates (PHAs) biosynthesis: insights from the recombinant Escherichia coli, J. Biotechnol. 180 (2014) 52–65.
[5] B. Younes, Classification, characterization, and the production processes of biopolymers used in the textiles industry, J. Textil. Inst. 108 (5) (2017) 674–682.
[6] M. Thielen, Bioplastics - Basics. Applications. Markets, Polymedia Publisher GmbH, Mönchengladbach, Germany, 2012.
[7] R. Hufenus, et al., Melt-spun fibers for textile applications, Materials 13 (19) (2020).
[8] E. Perret, et al., Structural response of melt-spun poly(3-hydroxybutyrate) fibers to stress and temperature, Polymer 197 (2020) 122503.
[9] E. Perret, et al., Tensile study of melt-spun poly(3-hydroxybutyrate) P3HB fibers: reversible transformation of a highly oriented phase, Polymer 180 (2019) 121668.
[10] H. Wang, K. Tashiro, Reinvestigation of crystal structure and intermolecular interactions of biodegradable poly(3-hydroxybutyrate) α-form and the prediction of its mechanical property, Macromolecules 49 (2) (2016) 581–594.
[11] R. Hufenus, et al., Molecular orientation in melt-spun poly(3-hydroxybutyrate) fibers: effect of additives, drawing and stress-annealing, Eur. Polym. J. 71 (2015) 12–26.
[12] E. Perret, R. Hufenus, Insights into strain-induced solid mesophases in melt-spun polymer fibers, Polymer 229 (2021) 124010.
[13] Y. Aoyagi, Y. Doi, T. Iwata, Mechanical properties and highly ordered structure of ultra-high-molecular-weight poly (R)-3-hydroxybutyrate films: effects of annealing and two-step drawing, Polym. Degrad. Stabil. 79 (2) (2003) 209–216.
[14] T. Iwata, et al., Processing of a strong biodegradable poly[(R)-3-hydroxybutyrate] fiber and a new fiber structure revealed by micro-beam X-ray diffraction with synchrotron radiation, Macromol. Rapid Commun. 25 (11) (2004) 1100–1104.
[15] T. Iwata, et al., Time-resolved X-ray diffraction study on poly (R)-3-hydroxybutyrate films during two-step-drawing: generation mechanism of planar zigzag structure, Biomacromolecules 6 (3) (2005) 1803–1809.
[16] T. Iwata, et al., Microbeam X-ray diffraction and enzymatic degradation of poly [(R)-3-hydroxybutyrate] fibers with two kinds of molecular conformations, Macromolecules 39 (17) (2006) 5789–5795.
[17] S. Phongtamrug, K. Tashiro, X-ray crystal structure analysis of poly(3-hydroxybutyrate) β-form and the proposition of a mechanism of the stress-induced α-to-β phase transition, Macromolecules 52 (8) (2019) 2995–3009.
[18] T. Kabe, et al., Investigating thermal properties of and melting-induced structural changes in cold-drawn P(3HB) films with alpha- and beta-structures using real-time X-ray measurements and high-speed DSC, Polymer 93 (2016) 181–188.
[19] B. Henrich, et al., PILATUS: a single photon counting pixel detector for X-ray applications, Nucl. Instrum. Methods Phys. Res. Sect. A Accel. Spectrom. Detect. Assoc. Equip. 607 (1) (2009) 247–249.
[20] E. Perret, et al., *WAXD, Polarized ATR-FTIR and DSC Data of Stress-Annealed Poly(3-Hydroxybutyrate) Fibers* Data in Brief, 2021 (under review).
[21] S.G. Kazarian, K.L.A. Chan, ATR-FTIR spectroscopic imaging: recent advances and applications to biological systems, Analyst 138 (7) (2013) 1940–1951.
[22] M.B. Huglin, M.A. Radwan, Behaviour of poly(β-hydroxybutyric acid) in dilute solution, Polym. Int. 24 (2) (1991) 119–123.
[23] E.M. Antipov, et al., Strain-induced mesophase and hard-elastic behaviour of biodegradable polyhydroxyalkanoates fibers, Polymer 47 (15) (2006) 5678–5690.
[24] T. Tanaka, et al., Formation of highly ordered structure in poly[(R)-3-hydroxybutyrate-co-(R)-3-hydroxyvalerate] high-strength fibers, Macromolecules 39 (8) (2006) 2940–2946.
[25] C.F. Macrae, et al., Mercury 4.0: from visualization to analysis, design and prediction, J. Appl.Cryst (2020) 53.
[26] J.L. Koenig, Chapter 4 - applications of IR spectroscopy to polymers, in: J.L. Koenig (Ed.), Spectroscopy of Polymers, second ed., Elsevier Science, New York, 1999, pp. 147–206.
[27] H.S. Barud, et al., Bacterial cellulose/poly(3-hydroxybutyrate) composite membranes, Carbohydr. Polym. 83 (3) (2011) 1279–1284.
[28] S. Bayarı, F. Severcan, FTIR study of biodegradable biopolymers: P(3HB), P(3HB-co-4HB) and P(3HB-co-3HV), J. Mol. Struct. 744–747 (2005) 529–534.
[29] C.M.S. Izumi, M.L.A. Temperini, FT-Raman investigation of biodegradable polymers: poly(3-hydroxybutyrate) and poly(3-hydroxybutyrate-co-3-hydroxyvalerate), Vib. Spectrosc. 54 (2) (2010) 127–132.
[30] J. Xu, et al., In situ FTIR study on melting and crystallization of polyhydroxyalkanoates, Polymer 43 (25) (2002) 6893–6899.
[31] S. Bloembergen, et al., Studies of composition and crystallinity of bacterial poly (β-hydroxybutyrate-co-β-hydroxyvalerate), Macromolecules 19 (11) (1986) 2865–2871.
[32] G. Lambeek, E.J. Vorenkamp, A.J. Schouten, Structural study of Langmuir-blodgett mono- and multilayers of poly(.beta.-hydroxybutyrate), Macromolecules 28 (6) (1995) 2023–2032.